

ANALYSIS OF FLOWING FLUID EFFECT ON FLOW AVERAGING TUBE

MIROSŁAW KABACIŃSKI*, CYPRIAN LACHOWICZ
AND JANUSZ POSPOLITA

*Opole University of Technology,
Mikołajczyka 5, 45-271 Opole, Poland
{m.kabacinski, c.lachowicz, j.pospolita}@po.opole.pl*

(Received 18 May 2008; revised manuscript received 29 May 2008)

Abstract: This paper presents a mathematical model and results of numerical simulations for a fluid flow around a flow averaging tube. The calculations have been performed using the commercially available FLUENT software. The authors have applied the currently known studies of the models of turbulence and their applicability in certain flow conditions and hence selected the RNG k - ε turbulence model including appropriate functions to be used for determination of pressures and velocities at the sites of occurrence of considerable gradients. The distributions of pressures and velocities around a sensor are presented along with pressure distributions, instantaneous and averaged in time, on the measuring tube surface. The paper determines the frequencies of measuring tube free vibrations for one sided and two-sided tube fitting for the tube length in the range 100–1500 mm. This analysis has been conducted with the aid of solving equations for free undamped vibrations for specific models. The graphical presentation involves an admissible range of tube lengths with one and two-sided fitting for the specified flowing air velocities.

Keywords: flow averaging tubes, numerical simulations, flow measurements

1. Introduction

Probes used for averaging dynamic pressure containing differential pressure transducers (Figure 1) tend to be applied as flowmeters in industrial applications, in particular in measurements of flows in pipelines with large diameters. This comes as a result of very competitive prices of such flowmeters in comparison to other technical solutions which can be applied for flow measurement. In addition, their fitting tends to be easier. The differential pressure transducers available in the market along with the option of considering the nonlinearity of characteristics offer an uncertainty level of measurement similar to the measurement error of other flowmeters.

One of the problems in the application of probes is associated with vibrations and the strain hazard, particularly in case of a flowmeter large length concurrent with a high velocity of the flow around the probe. Such vibrations affect the measurement

* Corresponding author

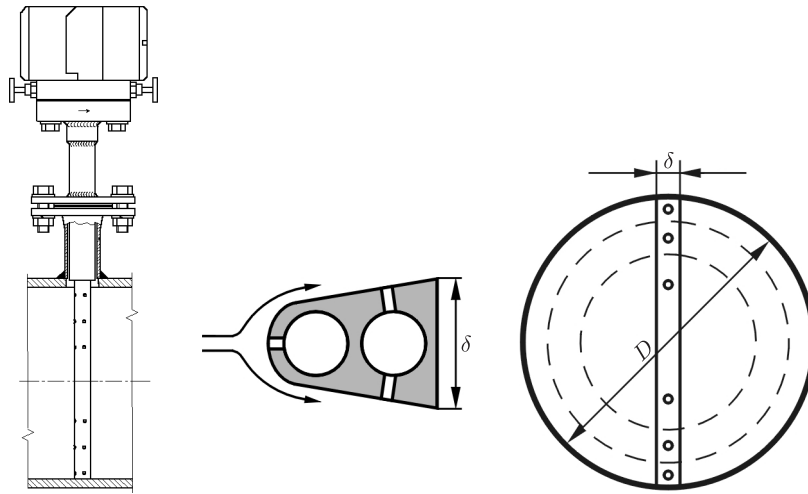


Figure 1. Flowmeter containing probe averaging dynamic pressure in pipe diameter

range limitation and result in increased uncertainty of measurement. For this reason, manufacturers of flowmeters determine the applicability to the flow measurement in specific pipeline cross sections and flowmeter fitting techniques. The fitting details lead to excluding the circumstances in which the frequency of dynamic effects approaches the frequency of sensor vibrations. The frequency of vibrations is determined on the basis of measurement (*e.g.* as a result of tensometric determination of the periodically variable force affecting the sensor), or otherwise it is based on the Strouhal number determined on the basis of the frequency of the forming vortices. Sample information regarding two profiles can be found in paper [1]. However, it has to be borne in mind that the sensor surrounding flow forms a physically complex phenomenon and the fluid's effect on the sensor is of a three-dimensional and non-stationary nature due to the formation of vortices. Hence, the paper undertakes an attempt at mathematical modeling and numerical simulation of the phenomenon [2].

2. Mathematical model of flow surrounding probe

This analysis involves a turbulent, unsteady (2D) viscous flow of an incompressible fluid. With the assumption of air velocities not exceeding 30 m/s, the fluid incompressibility assumption is justified. The mathematical model has been described with the motion equations for the velocity vector's U_i components:

$$\rho \frac{\partial \bar{U}_i}{\partial t} + \frac{\partial(\rho \bar{U}_i \bar{U}_j)}{\partial x_j} = -\frac{\partial p}{\partial x_i} + \frac{\partial}{\partial x_j} \left[\mu_{\text{ef}} \left(\frac{\partial \bar{U}_i}{\partial x_j} + \frac{\partial \bar{U}_j}{\partial x_i} \right) \right], \quad (1)$$

and in the following continuity equation:

$$\frac{\partial(\rho \bar{U}_i)}{\partial x_i} = 0. \quad (2)$$

In the above equations \bar{U}_i is a component of the velocity vector in the respective directions x and y , p – total pressure, ρ – fluid density. μ_{ef} is the effective viscosity which constitutes the total molecular viscosity μ and turbulent viscosity μ_t , *i.e.*

$$\mu_{\text{ef}} = \mu + \mu_t. \quad (3)$$

The turbulent viscosity is determined on the basis of the k - ε turbulence model [3]:

$$\mu_t = \rho C_\mu \frac{k^2}{\varepsilon}, \quad (4)$$

in which C_μ is equal to 0.0845 in case of the RNG k - ε model for the developed turbulence. The kinetic energy of turbulence k and the velocity of its dissipation ε are determined on the basis of the transport equations which take the following form in case of the RNG k - ε model:

$$\frac{\partial k}{\partial t} + \bar{U}_i \frac{\partial k}{\partial x_j} = \frac{1}{\rho} \frac{\partial}{\partial x_j} \left(\alpha_k \mu_{\text{ef}} \frac{\partial k}{\partial x_j} \right) + \frac{\mu_t}{\rho} \left(\frac{\partial \bar{U}_i}{\partial x_j} + \frac{\partial \bar{U}_j}{\partial x_i} \right) \frac{\partial \bar{U}_i}{\partial x_j} - \varepsilon, \quad (5)$$

$$\begin{aligned} \frac{\partial \varepsilon}{\partial t} + \bar{U}_i \frac{\partial \varepsilon}{\partial x_j} = & \frac{1}{\rho} \frac{\partial}{\partial x_j} \left(\alpha_\varepsilon \mu_{\text{ef}} \frac{\partial \varepsilon}{\partial x_j} \right) + \\ & \frac{C_1 \mu_t \varepsilon}{\rho k} \left(\frac{\partial \bar{U}_i}{\partial x_j} + \frac{\partial \bar{U}_j}{\partial x_i} \right) \frac{\partial \bar{U}_i}{\partial x_j} - \left(C_{2\varepsilon} + \frac{C_\mu \rho \eta^3 (1 - \eta/\eta_0)}{1 + \beta \eta^3} \right) \frac{\varepsilon^2}{k}. \end{aligned} \quad (6)$$

In the above equations α_k and α_ε denote the inverse effective Prandtl number for k and ε , respectively, for the higher Re ($\mu/\mu_{\text{ef}} \ll 1$) $\alpha_k = \alpha_\varepsilon \approx 1.393$, $\eta \equiv \frac{S_k}{\varepsilon}$ (S_k – user defined source in [4]), $\eta_0 = 4.38$, $\beta = 0.012$.

Equations (1)–(6) form a self-contained system which describes the discussed flow conditions. The above system is supplemented with boundary and initial conditions in respect to particular variables. The calculations area and the conditions at its boundaries are presented in Figure 2. The initial conditions have been assumed to take the form of such distributions of variables in the calculation area as those in the inflow cross section.

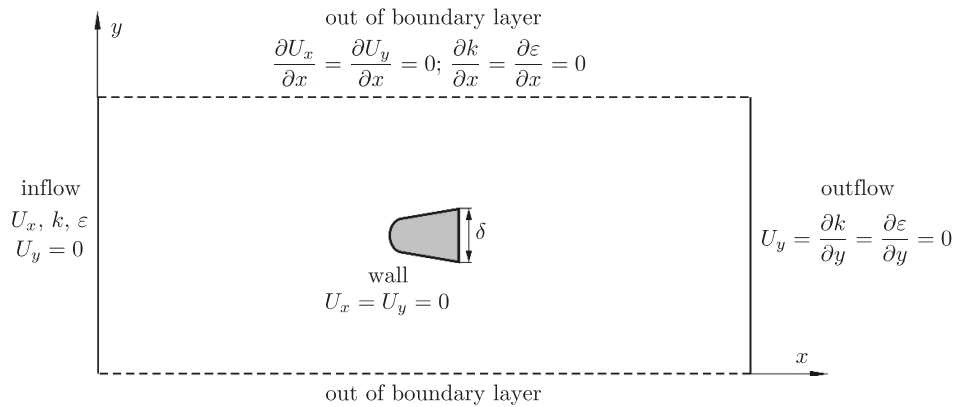


Figure 2. Boundary conditions for analyzed flow system

The boundary conditions for k and ε on the rigid walls result from the applied version of the k - ε model [4].

The mathematical model equations have been solved using the Finite Volume Method with the FLUENT software package [4]. The calculation area discretization has been conducted with the GAMBIT program [5].

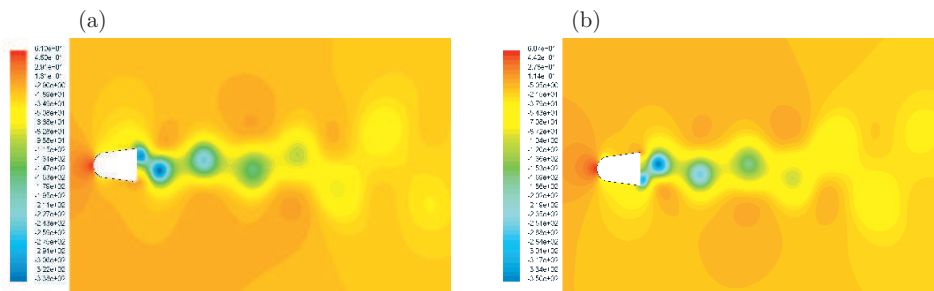


Figure 3. Distribution of static pressures [Pa] for the inflowing air stream velocity of 10 m/s for two selected time instances (a) t_1 and (b) t_2

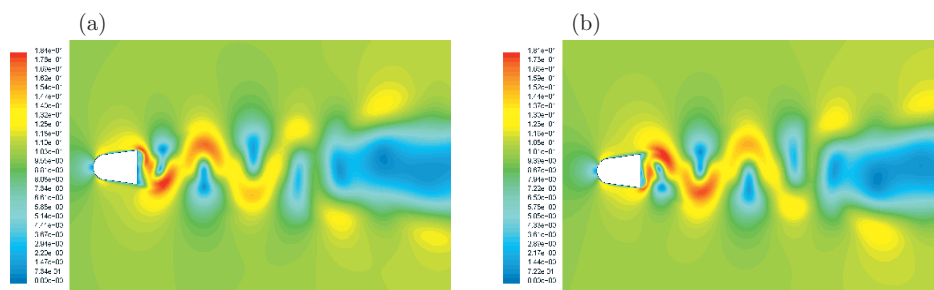


Figure 4. Distribution of velocities [m/s] around the sensor for two selected time instances (a) t_1 and (b) t_2 with inflowing air stream velocity of 10 m/s

3. Results of calculations

Figures 3 and 4 contain distributions of static pressures and distributions of magnitude velocities (numeric values) during the flow around the analyzed profiles for two selected time instances.

The vortex path is clearly discernible as it is generated by the profile. This path is generated outside the tapping pressure points which leads to the virtually unchanged pressure difference Δp . The largest differences of pressure and velocity with time are encountered behind the outflow surface of the profile.

The generated vortex path results in the fluid's periodical influence on the sensor in the flowmeter. The frequency range which is not concordant with the frequency of the installed flowmeter's vibrations results in a hazard of not only a deterioration of meteorological properties but a sensor failure, as well. Hence, the manufacturers of this type of flowmeters offer flow velocity ranges for specific flowmeters. Alternatively, the conditions regarding the fitting can be stated (one-sided and two-sided). Sometimes it is also the case that some requirements are stated regarding the selection of a particular sensor type (cross-sectional area) [3, 6, 7].

Figure 5 contains the averaged distribution of static pressures on the researched profile's surface and the distributions of the value for a few instants as the vortex path is generated. The results indicate that the considerable changes of physical properties with time which characterize the medium's flow occur mostly near the back wall of the examined profile. The fluctuations of pressure in this area display pulsatile characteristics with high amplitudes, but the duration of fluctuations is short. Hence, a considerable difference between the selected instantaneous distributions and

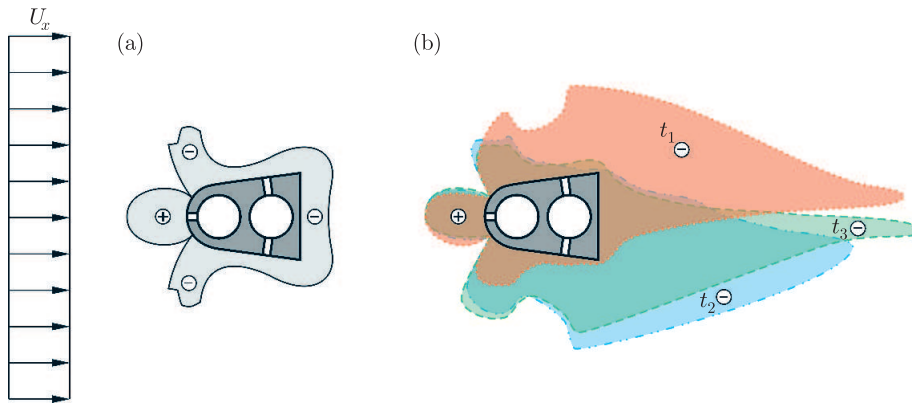


Figure 5. Distributions of static pressures relative to the inflowing air stream dynamic pressure with the velocity of 20 m/s: (a) averaged in time, (b) variable in time – for 3 selected time values t ($t_2 - t_1 = 1.16 \cdot 10^{-3}$ s; $t_3 - t_2 = 5.7 \cdot 10^{-4}$ s)

the mean distribution. Figure 6 contains the relation between the Strouhal number, $Sh = \frac{f \cdot \delta}{w}$, and the Reynolds number, $Re = \frac{w \cdot \delta}{\nu}$. For both numbers the characteristic dimension δ takes the form of the sensor back wall width ($\delta = 25\text{mm}$), f is the vortex generation frequency, w – the averaged flow velocity. The Strouhal number varies to a negligible extent which indicates a proportional frequency of the vortex separation from the medium flows velocity around the profile.

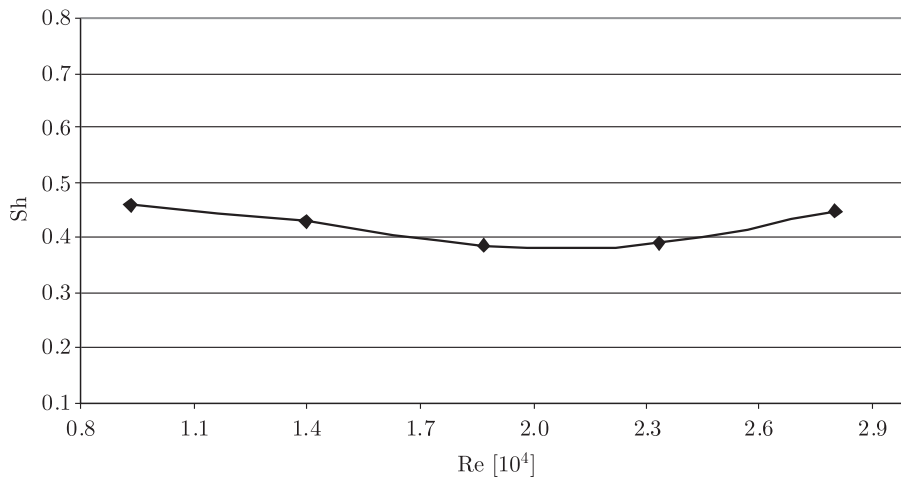


Figure 6. Strouhal number for surrounding flow sensor in Reynolds number function

4. Determination of probe free vibrations

An analysis of free vibrations has been conducted by solving the equations of free undamped vibrations for the system:

$$m\ddot{u}(t) + ku(t) = 0, \tag{7}$$

where u , \ddot{u} are the displacement and acceleration of the examined mass m , respectively, while k is the elasticity coefficient.

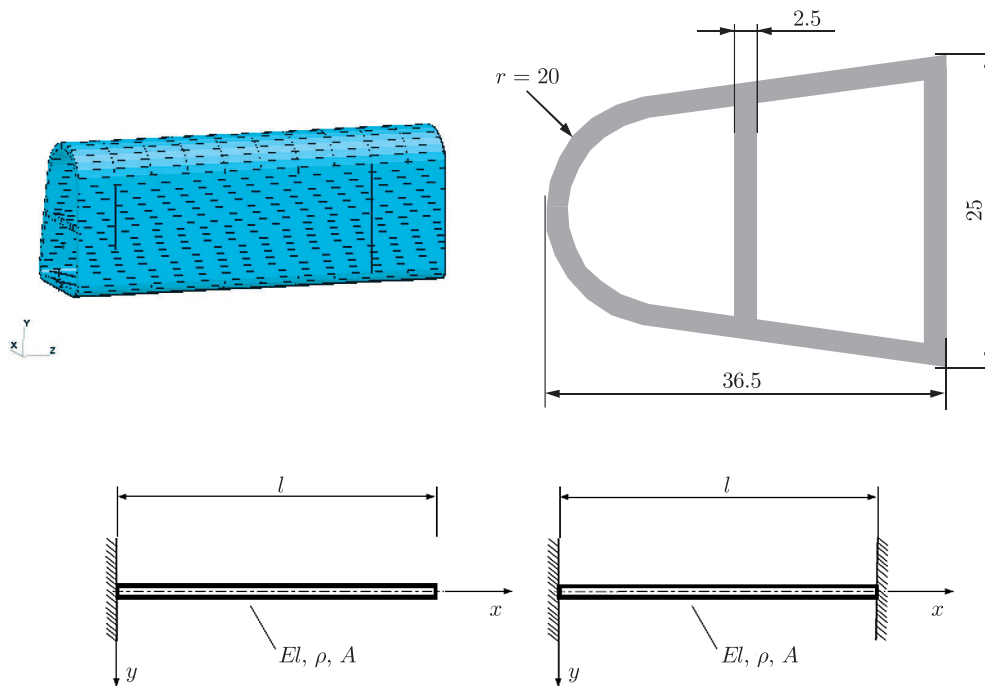


Figure 7. Adopted mesh across a probe section and examined fitting points

For the system presented in Figure 7 and applying the Finite Element Method (FEM) [8] it is necessary to solve a system of differential equations recorded in the form of a matrix [9]:

$$[M]\{\ddot{u}\} + [K]\{u\} = 0, \quad (8)$$

where $[M]$ is the mass matrix, $[K]$ – the stiffness matrix.

Figure 8 presents a tube model in a flowmeter considered as a vibrating system having n degrees of freedom. The vibrations of such a system are described with a system of Equations (8).

If the FEM software is applied to the development and solution of a system of Equations (8), the development of a mass matrix $[M]$ and a stiffness matrix of the entire structure is realized automatically on the basis of a geometrical model and the basic properties of the considered matter. Since the calculations are linear and elastic, it is sufficient to give the value of the Young's modulus, E , and Poisson constant, ν , of the material in the probe.

The vectors $\{\ddot{u}\}$ and $\{u\}$ in the system of Equations (8) are discrete sets of accelerations and displacement of particular nodes of the structure.

In order to solve the system of Equations (8) a specific solution form is assumed:

$$\{u\} = \{\phi\} \sin \omega t, \quad (9)$$

where $\{\phi\}$ is a set of eigenvectors, ω – circular frequency ($\omega = 2\pi f$).

An assumption of a harmonic shape of the solution to the system of Equations (9) leads to the observation that the free nodes of the structure are in a synchronized motion. This also means that the form of the structure's free vibrations

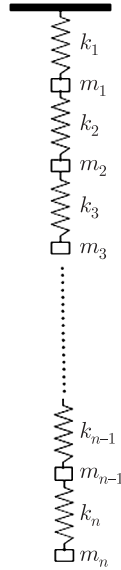


Figure 8. Vibrating system with n degrees of freedom (undamped)

is invariable in time and relative to the structure's geometrical co-ordination and assumed boundary conditions, *i.e.* the way in which the probe is fitted. Differentiating Equation (9) and substituting the result into Equation (8) the following form is obtained:

$$-\omega^2[M]\{\phi\}\sin\omega t + [K]\{\phi\}\sin\omega t = 0, \quad (10)$$

which can be simplified to take the form:

$$([K] - \omega^2[M])\{\phi\} = 0. \quad (11)$$

The above equation, sometimes called the eigenequation is a system of algebraic equations of components of eigenvectors $\{\phi\}$ and the corresponding eigenvalues ω . With the aid of the linear algebra methods the Equation (11) can be restated to take a form familiar from the theory of linear operators [10]:

$$[A - \lambda I]x = 0, \quad (12)$$

where A is the square matrix, λ - eigenvalue ($\omega^2 = \lambda$), I - unit matrix, x - eigenvector ($\{\phi\} = x$).

If matrix determinant $([K] - \omega^2[M]) = 0$, then there is a non-trivial solution $\{\phi\} \neq 0$. The determinant is equal to zero for the discrete set of eigenvalues ω_i^2 and the corresponding eigenvectors $\{\phi_i\}$. The particular eigenvalues and eigenvectors have concordant frequencies of the free vibrations ($f_i = \omega_i/2\pi$) and forms of free vibrations modes.

However, it has to be borne in mind that the calculated numeric values describing the geometrical form of vibrations modes are relative values, and hence they are scaled. The resulting values must not be associated with the observable displacements of the structure, but only with the observable forms of vibrations.

5. Results of calculations of frequencies of free vibrations of the probe

Tables 1 and 2 present the values of free vibrations [Hz] for one-sided and two-sided probe fitting, respectively.

Table 1. Frequencies of first five modes of free vibrations [Hz] for one-sided probe fitting

No.	length [mm]	mode 1 [Hz]	mode 2 [Hz]	mode 3 [Hz]	mode 4 [Hz]	mode 5 [Hz]
1	100	2223.0	2892.0	5159.0	7443.0	8336.0
2	200	596.0	809.8	3236.0	3293.0	4048.0
3	300	268.5	368.0	1573.9	2069.1	2239.4
4	400	151.5	208.6	914.3	1225.9	1688.4
5	500	97.1	133.9	593.9	804.7	1352.6
6	600	67.5	93.2	415.8	566.8	1129.2
7	700	49.6	68.5	306.9	420.0	842.8
8	800	37.9	52.4	235.7	323.4	650.2
9	900	30.0	41.5	186.6	256.5	516.4
10	1000	24.3	33.6	151.4	208.3	419.9
11	1100	20.1	27.8	125.3	172.6	347.9
12	1200	16.8	23.4	105.3	145.2	292.9
13	1300	14.4	20.0	89.8	123.8	250.0
14	1400	12.4	17.2	74.4	106.9	215.8
15	1500	10.8	14.9	67.5	93.2	188.2

Table 2. Frequencies of first five modes of free vibrations [Hz] for two-sided probe fitting

No.	length [mm]	mode 1 [Hz]	mode 2 [Hz]	mode 3 [Hz]	mode 4 [Hz]	mode 5 [Hz]
1	100	7888.0	8906.0	9723.0	10610.0	10910.0
2	200	3155.0	3921.0	5394.0	6658.0	7513.0
3	300	1567.0	2034.0	3823.0	4211.0	4763.0
4	400	918.8	1221.0	2358.0	3027.0	3294.0
5	500	599.0	807.0	1577.0	2067.0	2671.0
6	600	420.0	570.0	1122.0	1491.0	2107.7
7	700	310.0	424.0	836.6	1122.0	1588.0
8	800	239.0	326.9	646.7	873.3	1237.0
9	900	189.0	259.6	514.3	697.8	988.8
10	1000	153.7	211.1	418.5	569.8	807.6
11	1100	127.2	174.8	347.0	473.8	671.5
12	1200	106.9	147.2	292.3	399.9	566.9
13	1300	91.2	125.6	249.6	342.0	484.78
14	1400	78.0	108.5	215.5	295.7	419.1
15	1500	68.6	94.6	188.0	258.3	365.9

It can be concluded from the tables that the frequencies of free vibrations tend to decrease with the increasing probe length. The vibrations comprise an exploitation problem for larger probe lengths when the frequency of free vibrations overlaps with the frequency of periodically separating vortices. This is the way in which the fluid affects the sensor in a dynamic way. The possibilities associated with the limitation of the impact of this effect are associated with a change in the technique of probe fitting from one-sided to two-sided. An alternative is connected with a change in the probe cross section to take the form of a similar geometry; however, it needs to display a higher inertia mode.

Figure 9 contains the velocities of a medium in which case the separation frequency of vortices corresponds to the first harmonic of the free vibrations.

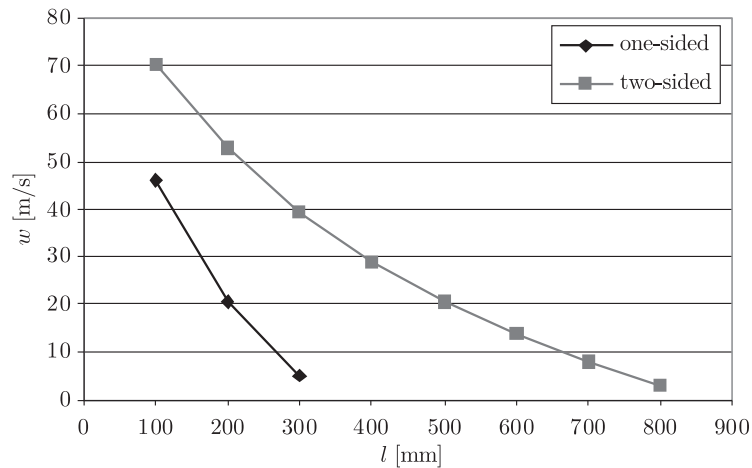


Figure 9. Range of admissible lengths of probe for particular velocities of medium

The above chart shows that one-sided fitting and a relatively high velocity of the medium are possible in the case of short sensors 100–200 mm in length. Longer probes will require two-sided fitting. In respect of application of sensors in channels with large diameters it is necessary both to apply the two-sided fitting and to increase the sensor's cross-sectional area.

6. Summary

The paper presents a mathematical model of a flow of a viscous fluid around a flow averaging tube along with the results of calculations. The phenomenon of generation of vortices has been observed in a tube section behind the probe which can lead to probe vibrations resulting from periodically variable distributions of pressures. This is particularly relevant for the case when the frequency of separation of vortices overlaps with the free vibrations of the sensor. The methodology used for determining these vibrations is presented and the vibrations for a particular probe averaging dynamic pressure type are determined [11]. The range of the operating conditions for probes is presented for the case when the frequency of the generated vortices is under the frequency of free vibrations. The above issues are particularly relevant for flow measurements in channels with large diameters.

Acknowledgements

This research paper was funded from the 2007–2008 science budget as a research project.

References

- [1] Sydencham P H and Dudziewicz J 1990 *The Handbook of Metrology*, Wydawnictwo Komunikacji i Łączności, Warsaw (in Polish)
- [2] Dobrowolski B, Kabaciński M and Pospolita J 2005 *Flow Measurement and Instrumentation* **16** (4) 251
- [3] Accutube, *Technical Documentation*, <http://www.accutube.com/>
- [4] 2005 *FLUENT 6.1.22. Fluid Dynamics Analysis Package*, Fluid Dynamics International, Inc.
- [5] 2005 *GAMBIT 2.2.30. Fluid Dynamics Analysis Package*, Fluid Dynamics International, Inc.
- [6] 1991 *Flow Measurement: Practical Guides for Measurement and Control* (Spitzer D W, Ed.), ISA, Research Triangle Park
- [7] Preso, *Technical Documentation*, <http://www.preso.com/>
- [8] Zienkiewicz O C and Taylor R L 2000 *The Finite Element Method*, 5th Edition, Butterworth-Heinemann, **I,II,III**
- [9] Szmelter J 1980 *Computer Methods in Mechanics*, *Biblioteka Naukowa Inżyniera*, PWN, Warsaw, p. 293 (in Polish)
- [10] Ralston A 1983 *Introduction to Numerical Analysis*, PWN, Warsaw, p. 536 (in Polish)
- [11] 2000 *Intról – Corporate Catalogue, Control-Measurement Apparatus*, Katowice